

Energy-composition relations in $\text{Ni}_3(\text{Al}_{1-x}\text{X}_x)$ phases, relevant to precipitation in nickel superalloys

Nikolai A. Zarkevich,¹ Timothy M. Smith,² John W. Lawson¹

¹ Intelligent Systems Division, NASA Ames Research Center, Moffett Field, CA 94035, USA

² NASA Glenn Research Center, 21000 Brook Park Rd., Cleveland, OH 44135, USA

Abstract:

Composition-structure-property dependencies provide useful insights for guided alloy design. Here we use density functional theory combined with the multiple scattering theory to compute dependencies of the structural energies and volumes (per atom) versus composition for ternary $\text{Ni}_3(\text{Al}_{1-x}\text{X}_x)$ alloys with $\text{X}=(\text{Ti}, \text{Zr}, \text{Hf}; \text{V}, \text{Nb}, \text{Ta}; \text{Cr}, \text{Mo}, \text{W})$ in L1_2 , D0_{24} , and D0_{19} phases with a homogeneous chemical disorder on the $(\text{Al}_{1-x}\text{X}_x)$ sublattice. Our results provide a better understanding of the physics in Ni_3Al -based precipitates and facilitate design of next-generation nickel superalloys with precipitation strengthening.

Keywords: Energy-composition; Materials design; precipitation; strengthening; superalloys.

1. Introduction:

Computed compositional dependencies of the relative structural energies can be used to design multi-phase materials and alloys with improved thermomechanical properties (in particular, with better creep and higher strength).^{1,2} Recently it was shown³ that local phase transformations inside Ni_3Al -based precipitates improve creep at the elevated operation temperatures T in Ni -based superalloys used in jet engines. At high T , local phase transformations are assisted by atomic diffusion. Structural defects (such as stacking faults) interact with diffusing atoms and are stabilized by the local chemical composition. Attractive interactions result in energy reduction after diffusion of particular atoms types towards defects, which act as sinks. Stabilization of stacking faults inside L1_2 precipitates reduces creep and improves mechanical strength of Ni superalloys.^{4,5} The stacking of atomic layers in extrinsic and intrinsic stacking faults in the L1_2 phase locally looks like D0_{19} and D0_{24} structures, respectively. Consequently, the stacking fault energy correlates with the energy difference between the relevant structures. To provide guidance for alloy design, we computed the compositional dependences of these structural energies.

The relevant atomic structures are compared in Figure 1. They differ by the stacking of the atomic layers along the cubic $[111]$ (in L1_2) and hexagonal (hex) $[0001]$ directions (in D0_{19} and D0_{24} structures). The periodic stacking sequences are $[\text{AB}]$ in D0_{19} and $[\text{ABAC}]$ in D0_{24} ; both structures can be viewed locally as stacking faults within the $[\text{ABC}]$ stacking in the cubic L1_2 structure along the $[111]$ direction. In $\text{Ni}_3(\text{Al}_{1-x}\text{X}_x)$ alloys with chemical disorder on the $(\text{Al}_{1-x}\text{X}_x)$ sublattice, this sublattice is simple cubic in L1_2 , hexagonal close-packed (hcp) in D0_{19} , and double hcp (dhcp) in D0_{24} .

The computed structural formation energies and equilibrium volumes (per atom) are shown in Figure 2. Relative energies versus composition are in Figure 3. Known composition-property dependencies allow to improve alloys by compositional adjustment.

This article is organized as follows. Methods are described in section 2. Results and discussion (section 3) are followed by summary (section 4).

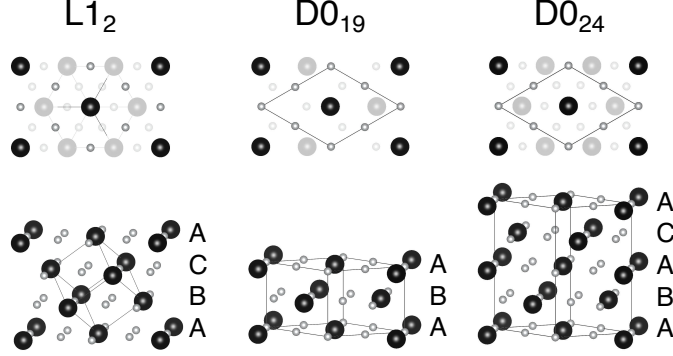


Fig. 1: Atomic structures of L1₂ (γ'), D0₁₉ (γ), and D0₂₄ (η) phases, shown for fully relaxed Ni₃Ti. The top panel shows cubic (111) and hexagonal (0001) projections, with shaded lower layers. The lower panel compares stacking of atomic layers. Ti is large black; Ni is small grey.

2. Methods:

We combine density functional theory (DFT) with multiple scattering theory (MST) to compute sets of energies⁶ of crystal structures with chemical disorder on sublattices. The homogeneous atomic disorder without a short-range order (SRO) is considered within the coherent potential approximation (CPA)⁷ in the Korringa-Kohn-Rostocker (KKR) formalism^{8,9}. The terminal binary Ni₃X structures are addressed by both KKR and full-potential DFT methods; the latter provides higher accuracy for structural formation energies, determined relative to the ground states of elemental solids. To get the advantages of both full-potential and MST methods, we use the full-potential formation energies of the terminal Ni₃X structures (see Table 1) and combine them with the KKR-CPA mixing energies of disordered Ni₃(Al_{1-x}X_x) structures. The mixing energies are defined relative to those of the terminal Ni₃X structures in the same phase. All equilibrium energies and volumes are computed at zero pressure and zero temperature $T = 0$ K; values are reported per atom, unless specified otherwise.

We use the all-electron KKR-CPA code¹⁰ to find mixing energies of Ni₃(Al_{1-x}X_x)₁ alloys with a homogeneous chemical disorder on the (Al_{1-x}X_x) sublattice. We use the full-potential VASP code¹¹ to compute formation energies of the fully ordered binary structures at the terminal Ni₃X compositions. In both codes we use the PBEsol¹² exchange correlation functional (XC=116133).

The KKR-CPA spin-polarized calculations⁷⁻⁹ were performed in primitive unit cells. We used two k -point meshes for the Brillouin Zone (BZ) integration. The primary (secondary) k -mesh was $12 \times 12 \times 12$ ($8 \times 8 \times 8$) for the cubic L1₂, $8 \times 8 \times 4$ ($6 \times 6 \times 4$) for the hexagonal (hex) D0₂₄ with fixed $c/a = (8/3)^{1/2}$ (ideal), and $8 \times 8 \times 10$ ($6 \times 6 \times 6$) for the hexagonal D0₁₉ with fixed $c/a = (2/3)^{1/2}$ (ideal). We included s , p , d , and f orbitals ($l_{\max} = 3$) in the basis inside the atomic spheres. For contour integration in the complex plane, we fixed the bottom energy at or below $E_{\text{bot}} = -0.9$ Ry. We used the muffin-tin approximation with periodic boundary corrections. At each composition x , the equilibrium volume V_0 and the minimal energy E_0 were found by fitting the Birch-Murnaghan^{13,14} equation of state (EOS) defining the energy versus volume $E(V)$ relation to 5 DFT points ($N_{\text{eos}} = 5$) with 1.5% step in the lattice constant a . To check accuracy, we used the fitted linear $V_0(x)$ dependence in each Ni₃(Al_{1-x}Hf_x) phase and directly computed DFT energies $E[V_0(x)]$, which agreed with the EOS energies $E_0(x)$ within the DFT error bars.

The VASP code¹¹ was compiled with the C2NEB subroutine^{15,16}. A dense Γ -centered Monkhorst-Pack mesh¹⁷ with ≥ 60 k -points per inverse Angstrom (\AA) was used for the BZ integration. The plane-wave energy cutoff was increased to ENCUT=650 eV. We used Gaussian smearing (ISMEAR=0) with SIGMA=0.043 eV, corresponding to $k_B T$ at $T=500$ K, where k_B is the

Boltzmann constant. DFT energy was obtained by extrapolation to zero smearing. Stacking fault energies were computed in a supercell with 40\AA between the periodic stacking faults; the energy of an ideal crystal was computed in a primitive unit cell.

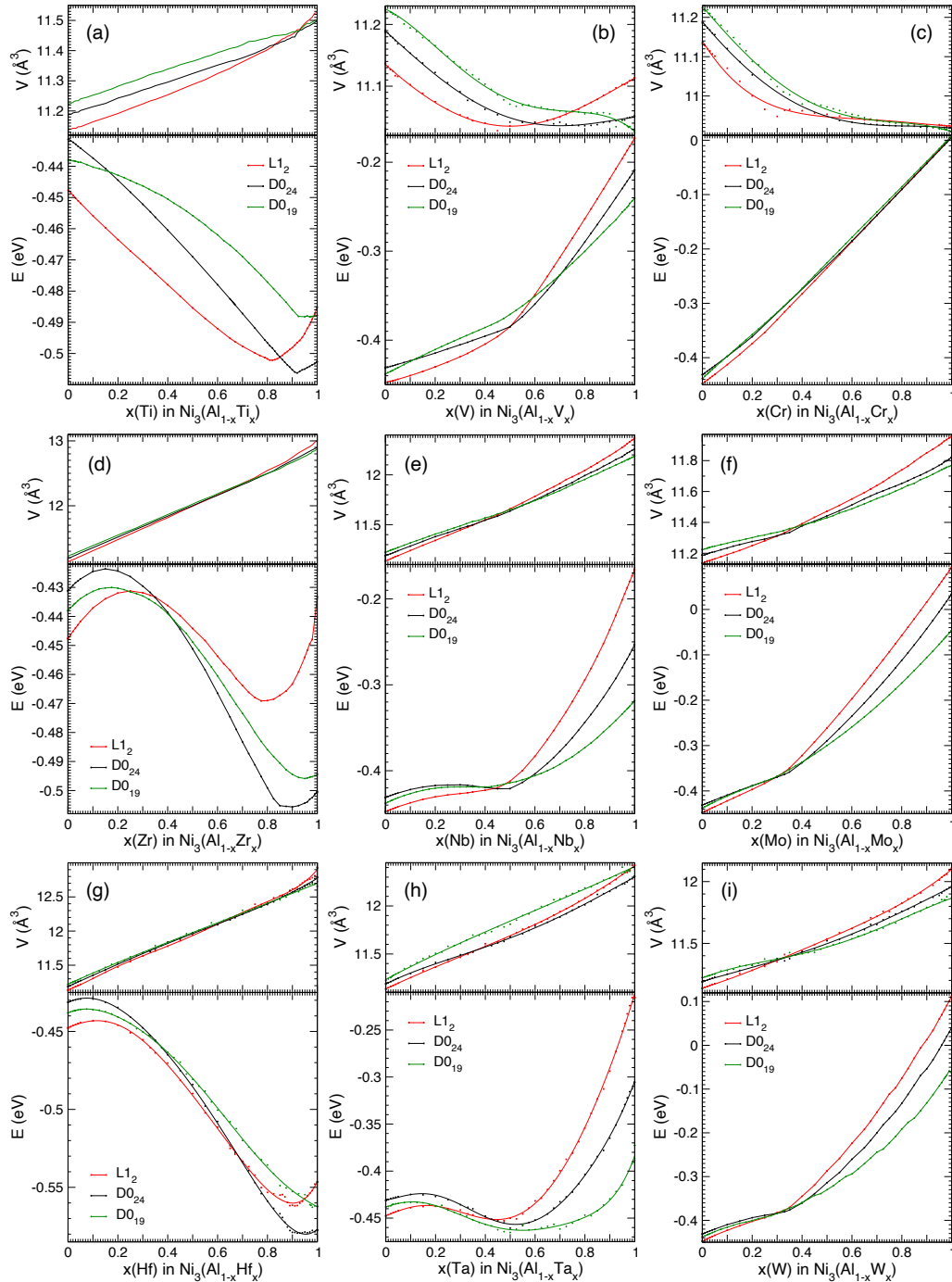


Fig. 2: Equilibrium volume V [$\text{\AA}^3/\text{atom}$] and formation energy E [eV/atom] of the $\text{Ni}_3(\text{Al}_{1-x}\text{X}_x)$ phases with homogeneous atomic disorder on the Al/X sublattice for group 4, 5, and 6 elements $X=(\text{Ti}, \text{Zr}, \text{Hf}; \text{V}, \text{Nb}, \text{Ta}; \text{Cr}, \text{Mo}, \text{W})$. The terminal formation energies of the binary Ni_3X alloys are from the full-potential VASP, while the relative mixing energies are from the KKR-CPA calculations. $L1_2$ is red, $D0_{24}$ is black, $D0_{19}$ is green.

3. Results:

Using density functional theory¹⁸⁻²⁰ and multiple scattering theory^{21,22}, we computed the equations of state, formation and mixing energies of the ordered Ni₃X and disordered Ni₃(Al_{1-x}X_x) alloys with X=(Ti, Zr, Hf; V, Nb, Ta; Cr, Mo, W) in L1₂, D0₁₉, and D0₂₄ phases, shown in Fig. 1. Formation energies (computed using VASP, relative to the ground states of elemental solids) of the terminal Ni₃X compositions are in Table 1. Mixing energies (relative to the ground states of the terminal Ni₃Al and Ni₃X compositions) were computed using KKR-CPA. Formation energies versus composition for the partially disordered Ni₃(Al_{1-x}X_x) structures (with a homogeneous disorder on the Al+X sublattice) are shown in Fig. 2. The EOS equilibrium energies E_0 and volumes V_0 are shown as dots. For X=(Hf, Ta) in Ni₃(Al_{1-x}Hf_x) and Ni₃(Al_{1-x}Ta_x), the $E(x)$ lines are the 6th degree polynomials, fitted to the EOS data points E_0 . For X=(Cr, W), the $V(x)$ lines are the 4th degree polynomials from the least-squares fit to the EOS volumes V_0 . For the other elements X, lines connect the computed EOS energies E_0 and volumes V_0 , shown as dots.

For completeness, we also provide relative energies ΔE in Fig. 3, which is complementary to Fig. 2. The differences ΔE are defined relative to $E_0(\text{L1}_2)$ at the same composition x . These differences $\Delta E(\text{D0}_{24} - \text{L1}_2) = E(\text{D0}_{24}) - E(\text{L1}_2)$ and $\Delta E(\text{D0}_{19} - \text{L1}_2) = E(\text{D0}_{19}) - E(\text{L1}_2)$ in Fig. 3 provide important additional information, while the shape of each $E(x)$ curve in Fig. 2 is related to the stability of each phase. The energy differences ΔE alone are not sufficient for materials design, especially if an unstable phase at some composition x transforms to another phase or segregates into other compositions. For example, $E_0(x)$ curves for all 3 phases of Ni₃(Al_{1-x}Zr_x)₁ alloys at $0 < x < 0.8$ point at a tendency to segregate into Zr-rich and Zr-deficient components; for a concave $E(x)$ dependency with a negative curvature such segregation would result in energy lowering.²³

Our first-principles calculations predict a change of the lowest-energy phase from L1₂ Ni₃Al to D0₂₄ for group 4 elements X=(Ti, Zr, Hf) and to D0₁₉ for group 5 elements X=(V, Nb, Ta), with a possible intermediate D0₂₄ phase for X=(V, Nb). These predictions agree with the experimental phase diagrams.²⁴

The equation of state contains equilibrium energy E_0 , volume V_0 , bulk modulus B_0 , and its dimensionless pressure derivative $B'_0 = \left(\frac{\partial B}{\partial P}\right)_T$ at constant temperature T . The computed values of B_0 and B'_0 in Table 2 were assessed from the EOS fitted to DFT KKR data. For the computed compositional dependences of B_0 and B'_0 we found that the differences between the linear and higher-degree polynomial approximations were within the error bars. Directly computed values of B_0 for Ni₃Al and Ni₃Ti in Table 2 can be compared with those at the terminal compositions from a linear fit of $B_0(x)$ for the Ni₃(Al_{1-x}Ti_x) system: $B_0(\text{L1}_2, x=0) = 193.13 \text{ GPa} \approx 193.1 \text{ GPa} = B_0(\text{L1}_2, \text{Ni}_3\text{Al})$; $B_0(\text{L1}_2, x=1) = 203.49 \text{ GPa} \approx 203.1 \text{ GPa} = B_0(\text{L1}_2, \text{Ni}_3\text{Ti})$; $B_0(\text{D0}_{24}, x=0) = 193.16 \text{ GPa} \approx 193.8 \text{ GPa} = B_0(\text{D0}_{24}, \text{Ni}_3\text{Al})$; $B_0(\text{D0}_{24}, x=1) = 204.92 \text{ GPa} \approx 204.7 \text{ GPa} = B_0(\text{D0}_{24}, \text{Ni}_3\text{Ti})$. The computed bulk modulus B_0 of L1₂ Ni₃Al is 193 GPa, and the experimental measurements range from 171 GPa²⁵ and 173.9 GPa²⁶ to 229.2 GPa²⁷. We conclude that our first-principles results reasonably agree with the available experimental data.

For changing composition x , magnetic and electronic structure changes in the Ni₃(Al_{1-x}Ti_x)₁ system.²⁸ Ni₃Al is magnetic, while Ni₃Ti is non-magnetic, with zero atomic magnetic moments, see Fig. 4 in Ref. 28. The rapid change of the electronic density of states at the Fermi energy E_F is responsible for the kink of the $E(x)$ curve in Ni₃(Al_{1-x}Ti_x)₁, present in each of the 3 phases. E_F is in the pseudo-gap in Ni₃Ti, but not in Ni₃Al, see Figs. 4 and 5. Ni₃(Al_{1-x}Ti_x)₁ crystal structure changes from L1₂ at smaller x to D0₂₄ at $x \geq 0.875$. Similar changes of electronic, magnetic, and atomic structure are also expected in other Ni₃(Al_{1-x}X_x)₁ systems.

The computed equation of state can be affected by a magnetic phase transition. This is the case, for example, in $D0_{19}$ Ni_3V : due to the disappearance of atomic magnetic moments near V_0 , the EOS fit of both magnetic states at $V > V_0$ and non-magnetic states at $V < V_0$ results in a larger fitting error and less accurate value of B'_0 . Two EOS fits of either non-magnetic states at $V < V_0$ (shown in Table 2) or magnetic states at $V > V_0$ provide two different equations of state with similar E_0 , but different B_0 and B'_0 values.

Our attempts to fit the EOS for the $D0_{19}$ (not the ground state) structure in Ni_3Mo and Ni_3W resulted in a large fitting error, originating from peculiarities of electronic structure. The equilibrium values of E_0 and V_0 were found reliably by energy minimization. However, the EOS fit of the higher-order terms B_0 and B'_0 was noisy: slightly different calculations provided different results. Ni_3Mo crystallized below $910^\circ C$ in the orthorhombic β - Cu_3Ti oP8 structure with $Pmmn$ space group (no. 59),²⁹ which was claimed to be stable.³⁰ Stability of Ni_3W oP8 structure³¹ is debatable³² and can be influenced by carbon.³³ Unstable Ni_3W $L1_2$ and $D0_{24}$ structures have positive formation energies (see Table 1 and Fig. 2), while Ni_3W $D0_{19}$ structure is not observed experimentally.³⁴ For comparison, the Cr-Ni system segregates into Cr and Ni solid solutions;³⁵ there are no stable Ni_3Cr compounds, in agreement with our calculations.

Fig. 2 allows to roughly estimate temperature-dependent solubility limits of dopants in the Ni_3Al $L1_2$ phase, using a rapid design estimate of phase-segregation temperature.³⁶ However, consideration of other phases, such as the orthorhombic $Ni_3(Nb_{0.8}Ti_{0.2})$ δ phase,³⁷ is beyond the scope of present work.

The Ti-rich $Ni_3(Al_{1-x}Ti_x)_1$ alloy was claimed²⁸ to be a compositional glass – an analogue of a spin glass in the compositional space. Such systems can be described by a truncated cluster expansion³⁸ with a degeneracy among the interactions³⁹ and frustration of the ground states.⁴⁰ At certain compositions x , we expect similarly frustrated ground states in several $Ni_3(Al_{1-x}X_x)_1$ systems.

Interestingly, in the $Ni_3(Al_{1-x}X_x)_1$ systems with $X=(Ti, V, Nb)$, the full-potential VASP calculations predict repulsion of $X=(Ti, V, Nb)$ from the stacking fault at small concentration x and attraction to the stacking fault at larger x . In particular, for $Ni_3(Al_{1-x}Nb_x)_1$, VASP results point at repulsion of Nb at small x from (attraction of Nb at larger x to) both intrinsic and extrinsic stacking faults. The KKR-CPA results in Fig. 3 indicate attraction of Nb to the stacking fault at larger x ; however, repulsion of Nb at small concentrations x from both intrinsic and extrinsic stacking faults was unexpected.⁴¹

In $L1_2$ Ni_3Nb (at $x=1$), the computed stacking fault energies are negative for both intrinsic and extrinsic stacking faults; this points at instability of $L1_2$ Ni_3Nb structure. Indeed, both $D0_{24}$ and $D0_{19}$ (the ground state of Ni_3Nb) structures are lower in energy than $L1_2$. At some composition x , a stacking fault energy changes its sign (i.e., becomes zero) in the $Ni_3(Al_{1-x}Nb_x)_1$ system.

In Ni_3Al (at $x=0$), our computed energy of the intrinsic stacking fault is 0.054 J/m²; this value reasonably agrees with those ranging from 0.037 to 0.092 J/m² in the literature.⁴¹⁻⁴⁸ Depending on the distance L between the periodic stacking faults in a supercell, the intrinsic stacking fault energy varies from 0.065 J/m² at $L \approx 10$ Å to 0.054 J/m² at $L > 40$ Å; a monotonic decrease of energy with distance at $L > 10$ Å points at repulsion between the stacking faults.

Stabilization of stacking faults in $L1_2$ precipitates reduces creep of Ni-based superalloys at high operating temperatures.³⁻⁵ Local phase transformation at stacking faults with increased concentration of dopants impedes propagation of additional dislocations along the stacking fault and thus improves creep resistance. The $D0_{24}$ and $D0_{19}$ structures locally look like $L1_2$ with periodic stacking faults, and the energy differences in Fig. 3 correlate with the stacking fault

energies. Thus, our results allow the engineering of stacking fault energies and improved creep in Ni superalloys by compositional adjustment. Discussion of a predictor for choosing the right chemical elements with appropriate concentrations that promote formation and stabilization of η (χ) phases along the superlattice intrinsic (extrinsic) stacking faults can be found in the literature.³⁻⁵ A limited amount of relevant DFT data can be found in Fig. 6 in Ref. 3. Here in Figs. 2 and 3 we show that the energy-composition relations are nonlinear. This detailed information can be used as an improved predictor, which takes into account the non-linearity of relative energies versus composition.

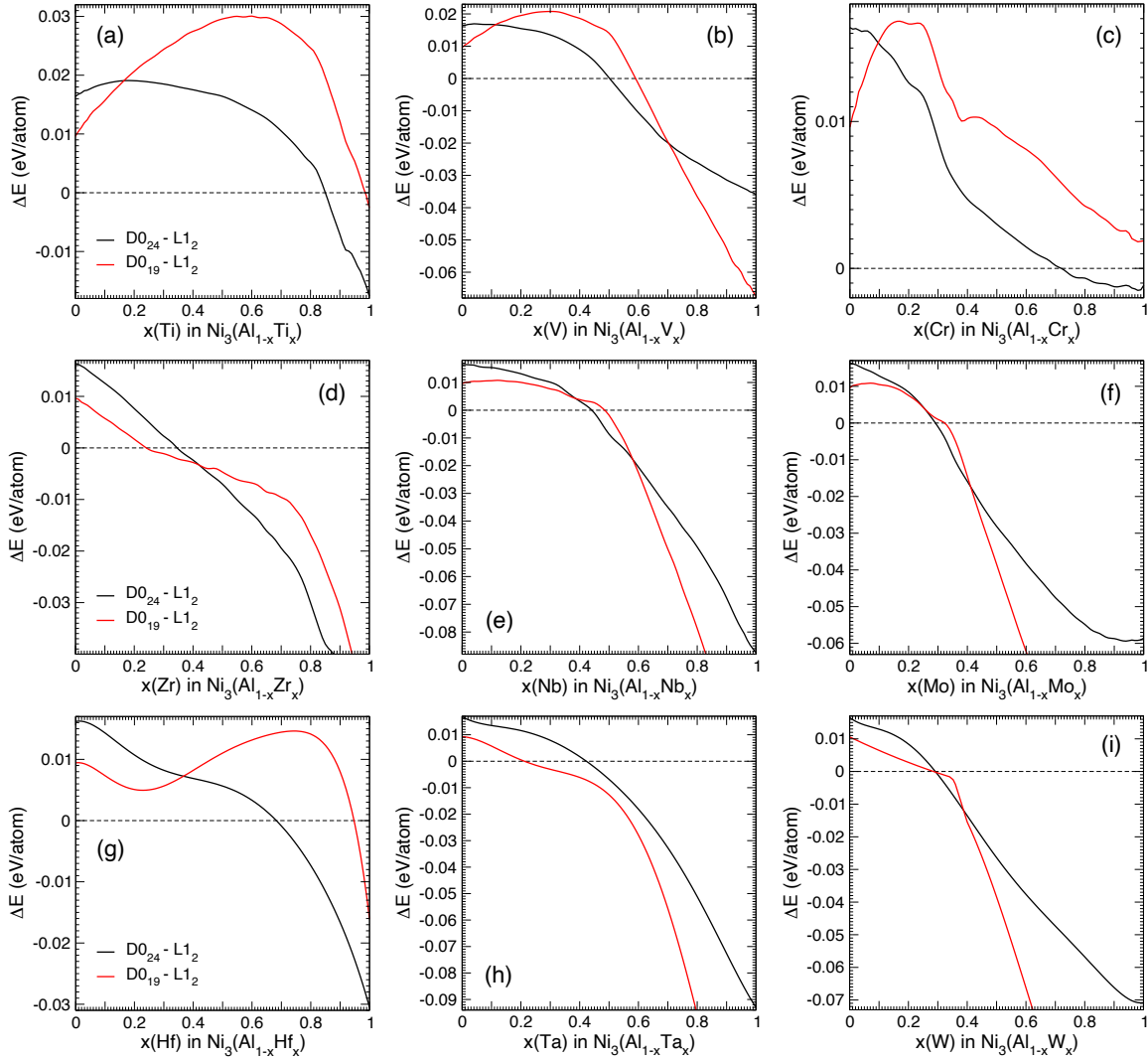


Fig. 3: Relative energies [eV/atom] of the $\text{Ni}_3(\text{Al}_{1-x}\text{X}_x)$ phases. Data in Fig. 2 was approximated by cubic splines and $E_0(\text{L}1_2)$ was subtracted. $\Delta E(\text{D}0_{24} - \text{L}1_2)$ is black and $\Delta E(\text{D}0_{19} - \text{L}1_2)$ is red.

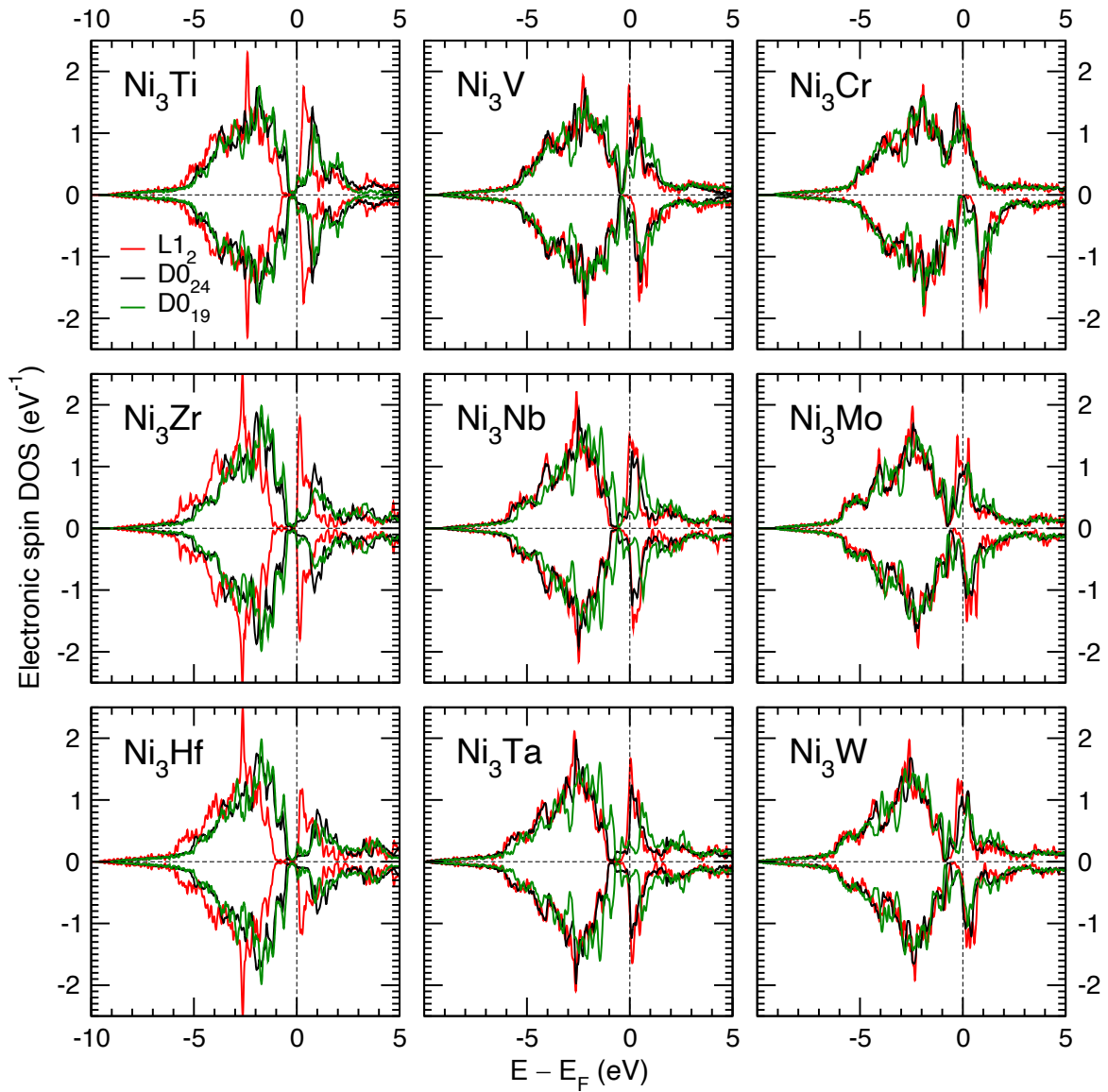


Fig. 4. Spin DOS in $L1_2$, $D0_{24}$ and $D0_{19}$ phases of Ni_3X compounds.

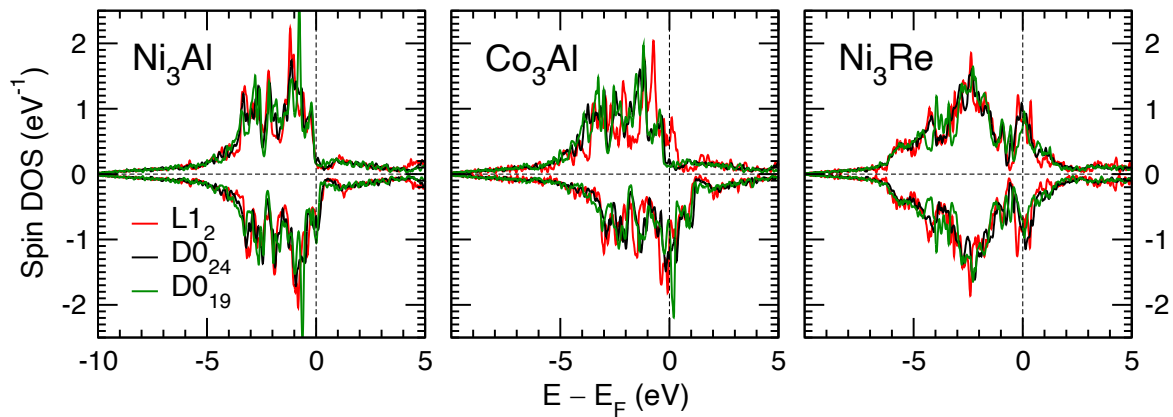


Fig. 5. Spin DOS in $L1_2$, $D0_{24}$ and $D0_{19}$ phases of Ni_3Al , Co_3Al , and Ni_3Re compounds.

Table 1. The computed formation energies [eV/atom] and volumes [$\text{\AA}^3/\text{atom}$] of Ni_3X compounds with L1₂, D0₁₉, and D0₂₄ structures, fully relaxed in VASP. The last column specifies the ground state (GS).

Ni_3X	E (eV/atom)			V ($\text{\AA}^3/\text{atom}$)			GS
	L1 ₂	D0 ₂₄	D0 ₁₉	L1 ₂	D0 ₂₄	D0 ₁₉	
Ni_3Al	-.4477	-.4313	-.4381	10.90	10.91	10.92	L1 ₂
Ni_3Ti	-.4852	-.5028	-.4878	11.25	11.24	11.25	D0 ₂₄
Ni_3Zr	-.4332	-.5007	-.4943	12.63	12.62	12.62	D0 ₂₄
Ni_3Hf	-.5465	-.5774	-.5621	12.37	12.34	12.35	D0 ₂₄
Ni_3V	-.1729	-.2088	-.2404	10.81	10.77	10.73	D0 ₁₉
Ni_3Nb	-.1658	-.2531	-.3184	11.99	11.92	11.88	D0 ₁₉
Ni_3Ta	-.2155	-.3054	-.3727	11.96	11.88	11.83	D0 ₁₉
Ni_3Cr	+.0062	+.0051	+.0081	10.66	10.64	10.60	other
Ni_3Mo	+.0924	+.0338	-.0460	11.59	11.49	11.46	other
Ni_3W	+.1124	+.0403	-.0593	11.62	11.53	11.49	other

Table 2. Computed EOS parameters: bulk modulus B_0 (GPa) and B'_0 (dimensionless) from KKR.

Ni_3X	B_0 (GPa)			B'_0		
	L1 ₂	D0 ₂₄	D0 ₁₉	L1 ₂	D0 ₂₄	D0 ₁₉
Ni_3Al	193.1	193.8	193.7	4.46	4.42	4.62
Ni_3Ti	203.1	204.7	204.6	4.51	4.47	4.36
Ni_3Zr	172.5	177.8	178.1	4.32	4.15	4.11
Ni_3Hf	182.8	175.0	192.5	4.36	4.27	4.23
Ni_3V	220.6	226.0	228.3	4.55	4.72	4.53
Ni_3Nb	207.0	213.1	217.7	4.32	4.42	4.49
Ni_3Ta	217.8	224.4	225.1	4.33	4.44	5
Ni_3Cr	214.6	216.4	217.8	5.02	4.96	5.04
Ni_3Mo	226.7	229.0	~238	4.42	4.41	4.47
Ni_3W	237.5	248.7	~270	4.56	4.20	4.2

4. Summary:

We have computed the compositional dependences of the equations of state, structural energies and volumes (per atom) for ternary $\text{Ni}_3(\text{Al}_{1-x}\text{X}_x)$ alloys with X=(Ti, Zr, Hf; V, Nb, Ta; Cr, Mo, W) in L1₂, D0₂₄, and D0₁₉ phases with disorder on the (Al_{1-x}X_x) sublattice. We considered both formation and relative energies and found their nonlinear dependencies versus composition. Our results allow better understanding of precipitation in multicomponent Ni superalloys. We hope that our *ab initio* data will be useful for designing next-generation superalloys with precipitation strengthening.⁴⁹

Acknowledgements: We acknowledge funding by NASA's Aeronautics Research Mission Directorate (ARMD) via Transformational Tools and Technologies (TTT) Project. We thank Anupa R. Bajwa, Mikhail Mendeleev, Valery V. Borovikov, and Shreyas J. Honrao for discussion.

Author contributions: Nikolai Zarkevich conceived the idea, performed calculations, and wrote the manuscript. Timothy Smith and John Lawson participated in discussions and editing.

References:

- 1 Jena, A. K. & Chaturvedi, M. C. The role of alloying elements in the design of nickel-base superalloys. *Journal of Materials Science* **19**, 3121-3139, doi:10.1007/BF00549796 (1984).
- 2 Reed, R. C. *The Superalloys: Fundamentals and Applications*. (Cambridge University Press, 2006).
- 3 Smith, T. M. *et al.* Utilizing local phase transformation strengthening for nickel-base superalloys. *Communications Materials* **2**, 106, doi:10.1038/s43246-021-00210-6 (2021).
- 4 Smith, T. M. *et al.* Segregation and η phase formation along stacking faults during creep at intermediate temperatures in a Ni-based superalloy. *Acta Materialia* **100**, 19-31, doi:10.1016/j.actamat.2015.08.053 (2015).
- 5 Smith, T. M. *et al.* Phase transformation strengthening of high-temperature superalloys. *Nature Communications* **7**, 13434, doi:10.1038/ncomms13434 (2016).
- 6 Zarkevich, N. A. Structural database for reducing cost in materials design and complexity of multiscale computations. *Complexity* **11**, 36-42, doi:10.1002/cplx.20117 (2006).
- 7 Johnson, D. D., Nicholson, D. M., Pinski, F. J., Gyorffy, B. L. & Stocks, G. M. Density-Functional Theory for Random Alloys: Total Energy within the Coherent-Potential Approximation. *Physical Review Letters* **56**, 2088-2091, doi:10.1103/PhysRevLett.56.2088 (1986).
- 8 Korringa, J. On the calculation of the energy of a Bloch wave in a metal. *Physica* **13**, 392-400, doi:10.1016/0031-8914(47)90013-X (1947).
- 9 Kohn, W. & Rostoker, N. Solution of the Schrödinger Equation in Periodic Lattices with an Application to Metallic Lithium. *Physical Review* **94**, 1111-1120, doi:10.1103/PhysRev.94.1111 (1954).
- 10 Johnson, D. D., Smirnov, A. V. & Khan, S. N. MECCA: Multiple-scattering electronic-structure calculations for complex alloys. KKR-CPA program. (Iowa State University and Ames Laboratory, Ames, Iowa, 2015).
- 11 Kresse, G. & Hafner, J. Ab initio molecular dynamics for liquid metals. *Phys Rev B* **47**, 558-561, doi:10.1103/PhysRevB.47.558 (1993).
- 12 Perdew, J. P. *et al.* Restoring the Density-Gradient Expansion for Exchange in Solids and Surfaces. *Physical Review Letters* **100**, 136406, doi:10.1103/PhysRevLett.100.136406 (2008).
- 13 Birch, F. Finite Elastic Strain of Cubic Crystals. *Physical Review* **71**, 809-824, doi:10.1103/PhysRev.71.809 (1947).
- 14 Murnaghan, F. D. The Compressibility of Media under Extreme Pressures. *Proceedings of the National Academy of Sciences* **30**, 244-247, doi:10.1073/pnas.30.9.244 (1944).
- 15 Zarkevich, N. A. & Johnson, D. D. Nudged-elastic band method with two climbing images: Finding transition states in complex energy landscapes. *The Journal of Chemical Physics* **142**, 024106, doi:10.1063/1.4905209 (2015).
- 16 Zarkevich, N. A. C2-NEB source code, <https://lib.dr.iastate.edu/ameslab_software/1/> (2014).
- 17 Monkhorst, H. J. & Pack, J. D. Special points for Brillouin-zone integrations. *Phys Rev B* **13**, 5188-5192, doi:10.1103/PhysRevB.13.5188 (1976).

- 18 Kohn, W. & Sham, L. J. Self-Consistent Equations Including Exchange and Correlation Effects. *Physical Review* **140**, A1133-A1138, doi:10.1103/PhysRev.140.A1133 (1965).
- 19 Martin, R. M. *Electronic Structure: Basic theory and practical methods*. (Cambridge University Press, 2004).
- 20 Martin, R. M., Reining, L. & Ceperley, D. M. *Interacting Electrons: Theory and Computational Approaches*. (Cambridge University Press, 2016).
- 21 Zarkevich, N. A. Theoretical and computational methods for accelerated materials discovery. *Modern Physics Letters B* **35**, 2130003, doi:10.1142/S0217984921300039 (2021).
- 22 Faulkner, J. S., Stocks, G. M. & Wang, Y. in *Electronic structure of solids* (IOP Publishing, 2018).
- 23 Yibole, H. *et al.* Manipulating the stability of crystallographic and magnetic sub-lattices: A first-order magnetoelastic transformation in transition metal based Laves phase. *Acta Materialia* **154**, 365-374, doi:10.1016/j.actamat.2018.05.048 (2018).
- 24 Massalski, T. B. *Binary Alloy Phase Diagrams*. 2nd edn, (ASM International, 1990).
- 25 Yasuda, H., Takasugi, T. & Koiwa, M. Elasticity of Ni-based L12-type intermetallic compounds. *Acta Metallurgica et Materialia* **40**, 381-387, doi:10.1016/0956-7151(92)90312-3 (1992).
- 26 Prikhodko, S. V., Yang, H., Ardell, A. J., Carnes, J. D. & Isaak, D. G. Temperature and composition dependence of the elastic constants of Ni₃Al. *Metallurgical and Materials Transactions A* **30**, 2403-2408, doi:10.1007/s11661-999-0248-9 (1999).
- 27 Pearson, W. B. & Raynor, G. V. *A Handbook of Lattice Spacings and Structures of Metals and Alloys*. (Elsevier, 2013).
- 28 Zarkevich, N. A., Smith, T. M., Baum, E. N. & Lawson, J. W. Compositional Glass: A State with Inherent Chemical Disorder, Exemplified by Ti-rich Ni₃(Al,Ti)₁ D0₂₄ Phase. *Crystals* **12**, 1049 (2022).
- 29 Casselton, R. E. W. & Hume-Rothery, W. The equilibrium diagram of the system molybdenum-nickel. *Journal of the Less Common Metals* **7**, 212-221, doi:10.1016/0022-5088(64)90068-2 (1964).
- 30 Wang, Y., Woodward, C., Zhou, S. H., Liu, Z. K. & Chen, L. Q. Structural stability of Ni–Mo compounds from first-principles calculations. *Scripta Mater* **52**, 17-20, doi:10.1016/j.scriptamat.2004.09.007 (2005).
- 31 Arapova, L. P. Crystalline structure of the intermetallic phases of WNi₃ and MoNi₃. *Soviet Physics Journal* **16**, 1173-1175, doi:10.1007/BF00890486 (1973).
- 32 Isomäki, I., Hämäläinen, M., Braga, M. H. & Gasik, M. First principles, thermal stability and thermodynamic assessment of the binary Ni–W system. *International Journal of Materials Research* **108**, 1025-1035, doi:doi:10.3139/146.111557 (2017).
- 33 Liu, X., Pilling, J., Heckel, R. W. & Lee, J. K. Influence of carbon on bond strength between nickel and Ni–W alloys. *Materials Science and Technology* **7**, 228-238, doi:10.1179/mst.1991.7.3.228 (1991).
- 34 Cury, R., Joubert, J. M., Tusseau-Nenez, S., Leroy, E. & Allavena-Valette, A. On the existence and the crystal structure of Ni₄W, NiW and NiW₂ compounds. *Intermetallics* **17**, 174-178, doi:10.1016/j.intermet.2008.11.001 (2009).

- 35 Nash, P. The Cr–Ni (Chromium-Nickel) system. *Bulletin of Alloy Phase Diagrams* **7**, 466-476, doi:10.1007/BF02867812 (1986).
- 36 Zarkevich, N. A., Tan, T. L. & Johnson, D. D. First-principles prediction of phase-segregating alloy phase diagrams and a rapid design estimate of their transition temperatures. *Phys Rev B* **75**, 104203, doi:10.1103/PhysRevB.75.104203 (2007).
- 37 Lyu, F. *et al.* The δ Phase Precipitation of an Inconel 718 Superalloy Fabricated by Electromagnetic Stirring Assisted Laser Solid Forming. *Materials* **12**, 2604 (2019).
- 38 Zarkevich, N. A. & Johnson, D. D. Reliable First-Principles Alloy Thermodynamics via Truncated Cluster Expansions. *Physical Review Letters* **92**, 255702, doi:10.1103/PhysRevLett.92.255702 (2004).
- 39 Zarkevich, N. A., Tan, T. L., Wang, L. L. & Johnson, D. D. Low-energy antiphase boundaries, degenerate superstructures, and phase stability in frustrated fcc Ising model and Ag-Au alloys. *Phys Rev B* **77**, 144208, doi:10.1103/PhysRevB.77.144208 (2008).
- 40 Mydosh, J. A. *Spin Glasses: An Experimental Introduction*. 1st edn, (CRC Press, 1993).
- 41 Rao, Y., Smith, T. M., Mills, M. J. & Ghazisaeidi, M. Segregation of alloying elements to planar faults in γ' -Ni₃Al. *Acta Materialia* **148**, 173-184, doi:10.1016/j.actamat.2018.01.055 (2018).
- 42 Schoeck, G., Kohlhammer, S. & Fahnle, M. Planar dissociations and recombination energy of [110] superdislocations in Ni₃Al: Generalized Peierls model in combination with ab initio electron theory. *Philosophical Magazine Letters* **79**, 849-857, doi:10.1080/095008399176544 (1999).
- 43 Mryasov, O. N., Gornostyrev, Y. N., van Schilfgaarde, M. & Freeman, A. J. Superdislocation core structure in L1₂ Ni₃Al, Ni₃Ge and Fe₃Ge: Peierls–Nabarro analysis starting from ab-initio GSF energetics calculations. *Acta Materialia* **50**, 4545-4554, doi:10.1016/S1359-6454(02)00282-3 (2002).
- 44 Wen, Y.-f., Sun, J. & Huang, J. First—principles study of stacking fault energies in Ni₃Al intermetallic alloys. *Transactions of Nonferrous Metals Society of China* **22**, 661-664, doi:10.1016/S1003-6326(11)61229-6 (2012).
- 45 Yu, X.-X. & Wang, C.-Y. The effects of alloying elements on generalized stacking fault energies, strength and ductility of γ' -Ni₃Al. *Materials Science and Engineering: A* **539**, 38-41, doi:10.1016/j.msea.2011.12.112 (2012).
- 46 Liu, L.-L., Wu, X.-Z., Wang, R., Li, W.-G. & Liu, Q. Stacking fault energy, yield stress anomaly, and twinnability of Ni₃Al: A first principles study*. *Chinese Phys B* **24**, 077102, doi:10.1088/1674-1056/24/7/077102 (2015).
- 47 Hasan, H., Mlkvik, P., Haynes, P. D. & Vorontsov, V. A. Generalised stacking fault energy of Ni-Al and Co-Al-W superalloys: Density-functional theory calculations. *Materialia* **9**, 100555, doi:10.1016/j.mtla.2019.100555 (2020).
- 48 Shang, S.-L. *et al.* Unveiling dislocation characteristics in Ni₃Al from stacking fault energy and ideal strength: A first-principles study via pure alias shear deformation. *Phys Rev B* **101**, 024102, doi:10.1103/PhysRevB.101.024102 (2020).
- 49 T.M. Smith *et al.* A 3D Printable Alloy Designed for Extreme Environments. *Nature* (2023).